Journal of Vacuum Science and Technology A

RESEARCH ARTICLE | SEPTEMBER 26 2023

Isotropic plasma-thermal atomic layer etching of superconducting titanium nitride films using sequential exposures of molecular oxygen and SF_6/H_2 plasma

Azmain A. Hossain ; Haozhe Wang ; David S. Catherall ; Martin Leung; Harm C. M. Knoops ; James R. Renzas ; Austin J. Minnich

J. Vac. Sci. Technol. A 41, 062601 (2023)
https://doi.org/10.1116/6.0002965
CHORUS

JVST A
Journal of Vacuum Science & Technology A
ARTICLE
pubs.aip.org/avs/jva

Isotropic plasma-thermal atomic layer etching of superconducting titanium nitride films using sequential exposures of molecular oxygen and SF_6/H_2 plasma

Cite as: J. Vac. Sci. Technol. A **41**, 062601 (2023); doi: 10.1116/6.0002965
Submitted: 13 July 2023 · Accepted: 10 August 2023 ·
Published Online: 26 September 2023

View Online Export Citation CrossMark

Azmain A. Hossain,[1] Haozhe Wang,[1] David S. Catherall,[1] Martin Leung,[2] Harm C. M. Knoops,[3,4] James R. Renzas,[3] and Austin J. Minnich[1,a)]

AFFILIATIONS

[1]Division of Engineering and Applied Science, California Institute of Technology, Pasadena, California 91125
[2]Division of Natural Sciences, Pasadena City College, Pasadena, California 91106
[3]Oxford Instruments Plasma Technology, North End, Bristol BS49 4AP, United Kingdom
[4]Department of Applied Physics, Eindhoven University of Technology, P.O. Box 513, 5600MB Eindhoven, The Netherlands

[a)]**Author to whom correspondence should be addressed:** aminnich@caltech.edu

ABSTRACT

Microwave loss in superconducting TiN films is attributed to two-level systems in various interfaces arising in part from oxidation and microfabrication-induced damage. Atomic layer etching (ALE) is an emerging subtractive fabrication method which is capable of etching with angstrom-scale etch depth control and potentially less damage. However, while ALE processes for TiN have been reported, they either employ HF vapor, incurring practical complications, or the etch rate lacks the desired control. Furthermore, the superconducting characteristics of the etched films have not been characterized. Here, we report an isotropic plasma-thermal TiN ALE process consisting of sequential exposures to molecular oxygen and an SF_6/H_2 plasma. For certain ratios of SF_6:H_2 flow rates, we observe selective etching of TiO_2 over TiN, enabling self-limiting etching within a cycle. Etch rates were measured to vary from 1.1 Å/cycle at 150 °C to 3.2 Å/cycle at 350 °C using *ex situ* ellipsometry. We demonstrate that the superconducting critical temperature of the etched film does not decrease beyond that expected from the decrease in film thickness, highlighting the low-damage nature of the process. These findings have relevance for applications of TiN in microwave kinetic inductance detectors and superconducting qubits.

I. INTRODUCTION

Titanium nitride (TiN) is a superconducting metal of interest for microelectronics and superconducting quantum devices. Its high kinetic inductance, low microwave loss, and high absorption coefficient in the infrared and optical frequencies make it a promising material for single photon detectors,[1,2] ultrasensitive current detectors,[3] quantum-limited parametric amplifiers,[4] and qubits.[5,6] Superconducting microwave resonators based on TiN routinely exhibit internal quality factors $Q_i > 10^6$.[2,6,7] TiN is also used for microelectronics applications in which it is employed as a copper diffusion barrier and metal gate electrode.[8–10] In many of these applications, imperfections at film interfaces are the primary limitation to figures of merit for various devices; for instance, the quality factor of superconducting microresonators is presently thought to be limited by microwave surface loss associated with two-level systems (TLS) in various interfaces.[11–13] Subtractive nanofabrication methods based on typical wet or dry etching processes are unsuitable for mitigating TLS density in these devices due to the lack of angstrom-scale precision in etching and the sub-surface damage they induce.[14–16]

Atomic layer etching (ALE) is an emerging subtractive nanofabrication process with potential to overcome these limitations.[17–19] Early forms of ALE focused on directional etching.[20,21] Directional ALE is based on surface modification by adsorption of reactive

species, and subsequent sputtering of the modified surface with ions or neutral atoms of low energy exceeding only the sputtering threshold of the modified surface.[22,23] Isotropic thermal ALE processes have also been developed recently using sequential, self-limiting surface chemical reactions.[24] In thermal ALE, the material surface is modified to form a nonvolatile layer that can then be removed by a selective mechanism, such as temperature cycling,[25,26] ligand-exchange transmetalation reactions,[24,27] or others.[18] Isotropic thermal and plasma ALE processes have now been reported for various dielectrics and semiconductors, including Al_2O_3,[28,29] SiO_2,[30,31] AlN,[32–34] InGaAs,[35,36] and others.[18,37–39] Surface smoothing of etched surfaces using ALE has also been reported for various metals and semiconductors.[28,36,40,41]

For TiN, ALE processes based on fluorination and ligand-exchange with $Sn(acac)_2$, trimethylaluminum (TMA), dimethylaluminum chloride, and $SiCl_4$ did not lead to etching.[42] When fluorinated, TiN retains its 3+ oxidation state, yielding TiF_3. TiF_3 either formed nonvolatile ligand-exchange products or did not react with the precursors, and hence, no etching occurred. This difficulty was overcome by first converting the Ti to the 4+ oxidation state with exposure to ozone or H_2O_2, which upon fluorination using HF produced volatile TiF_4.[43] A conceptually similar process has also been reported using O_2 plasma and CF_4 plasma.[44]

Despite these advances, limitations remain. The use of HF vapor incurs practical complications. The process of Ref. 44 based on O_2 plasma and CF_4 requires a heating and cooling step per cycle, which can lead to impractical time per cycle on conventional plasma tools. Additionally, the recipe achieves nm/cycle etch rates, which lacks the desired angstrom-scale control and low-damage characteristics. Previous reports did not examine the effects of ALE on the superconducting properties of the samples. Identifying alternate reactants to HF vapor while maintaining angstrom-level precision over the thickness and ensuring that superconducting properties are not degraded, all remain topics of interest for TiN ALE.

Here, we report the isotropic atomic layer etching of TiN using sequential exposures of O_2 gas and SF_6/H_2 plasma. The process is based on the selective etching of TiO_2 over TiN for certain ratios of SF_6:H_2. The observed etch rates varied from 1.1 up to 3.2 Å/cycle for temperatures between 150 °C and 350 °C, respectively, as measured using *ex situ* ellipsometry. The etched surface was found to exhibit a ~40% decrease in surface roughness. The superconducting transition temperature was unaffected by ALE beyond the expected change due to the decrease in film thickness, highlighting the low-damage nature of the process. Our findings indicate the potential of ALE in the processing of TiN for superconducting quantum electronics and microelectronics applications.

II. EXPERIMENT

The plasma-thermal ALE process of this work is illustrated in Fig. 1. An exposure of molecular oxygen was used to oxidize the surface of TiN to TiO_2, followed by a purge. Next, a mixture of SF_6 and H_2 gas was introduced into the chamber and ignited to form SF_6/H_2 plasma. After this exposure, the reactor was again purged to complete the cycle. The use of SF_6/H_2 plasma was motivated by noting that HF does not etch TiN, but fluorine radicals will spontaneously etch TiN.[43,45] Studies on SiN and Si etching using hydrogen and fluorine-containing plasma have shown that the plasma formed by the mixture yields different products at different plasma concentration ratios, including HF molecules at high hydrogen concentrations (H_2 to F-containing gas flow rate ratio $\gtrsim 2$).[46–48] We, therefore, expected to observe an effect similar to that reported in Refs. 46–48, in which fluorine radicals were found to combine with hydrogen radicals via multiple pathways to form vibrationally excited HF with negligible F radical concentration.[46] If this process did occur, the HF formed *in situ* could then react with the film and selectively etch TiO_2 over TiN, with minimal spontaneous etching from F radicals at sufficiently high H_2 concentrations. The etch selectivity of TiO_2 over TiN is due to the differing oxidation states of Ti in each compound, as previously observed in Ref. 43. The formation of HF in the SF_6/H_2 plasma is referred to as "*in situ* HF" throughout the paper. An SF_6 gas was used in this work because of its successful use in previous work on the isotropic ALE of alumina and aluminum nitride.[33,49]

We investigated this approach to ALE of TiN using an Oxford Instruments FlexAL atomic layer deposition (ALD) system with an inductively coupled plasma source, as described in Refs. 50 and 51. The substrate table temperature varied between 150 °C and 350 °C, as measured by the FlexAL substrate table thermometer. The minimum temperature in our study was restricted to 150 °C by the tool. The sample was placed on a silicon carrier wafer, which sits on the substrate table, which may cause a difference between the true sample temperature and the table temperature. Prior to introducing the sample into the chamber for etching, the chamber walls and the carrier wafer were conditioned by coating with 50 nm of Al_2O_3 using 300 cycles of Al_2O_3 ALD.[51] Alumina was selected as it does not form volatile fluoride species on exposure to SF_6 plasma. For

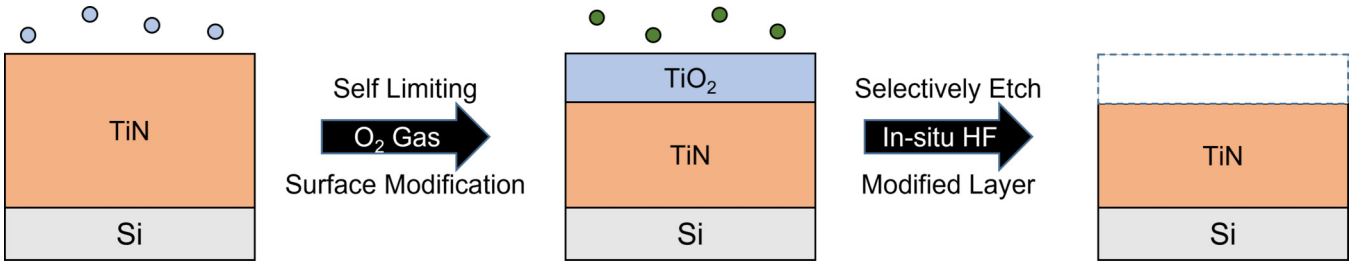

FIG. 1. Schematic of the TiN ALE process involving exposures to molecular oxygen to oxidize the surface (O_2, blue dots), followed by SF_6/H_2 plasma (green dots) to produce volatile etch products.

TiN ALE, the sample was first exposed to 50 sccm O_2 and 50 sccm Ar gas for 2 s at 100 mTorr pressure, followed by a 10 s purge. Next, a mixture of 20 sccm H_2 and 4 sccm SF_6 was stabilized at 100 mTorr for 5 s before striking the plasma at 100 W for 10 s. The excess reactants were purged for 10 s before repeating the cycle. The recipe resulted in a total time of ~40 s per cycle. Before the sample was moved to the loadlock, the chamber was pumped down for 60 s. The sample was additionally held in the loadlock for 2 h to cool down before exposure to air to reduce oxygen diffusion into the sample.

The film thickness before and after etching was measured by *ex situ* spectroscopic ellipsometry (J.A. Woolam M2000) at 60° and 70° from 370 to 1000 nm. Thickness was determined using 5 points on a $5 \times 5\,mm^2$ square array. Subsequently, the data were fit using a Lorentz model to obtain the thickness of the samples.[43,52] The thickness and uncertainty values are the average and standard deviation of the five points, respectively. XPS analysis was performed using a Kratos Axis Ultra x-ray photoelectron spectrometer using a monochromatic Al Kα source. Depth profiling was performed using an Ar ion beam with a 60 s interval for each cycle. The estimated milling depth was calculated based on the initial and final film thickness measured by *ex situ* ellipsometry and assuming a constant ion milling rate. The XPS data were analyzed in CASA-XPS from Casa Software Ltd. We adopt universal Tougaard background and subpeak fitting routines from Refs. 53 and 54.

The film surface topography was characterized using a Bruker Dimension Icon atomic force microscope (AFM) over a $0.25 \times 0.25\,\mu m^2$ area. The raw height maps collected on the AFM were processed by removing tilt via a linear plane-fit. The surface roughness and the power spectral density (PSD) were computed from the plane-fit height maps using procedures outlined in the previous literature.[41,55] The PSD provides a quantitative measure of the lateral distance over which the surface profile varies in terms of spatial frequencies.[55,56] The PSD was calculated by taking the absolute square of the normalized 1D-discrete Fourier transform of each row and column from the plane-fit AFM scan. The transformed data were then averaged to produce a single PSD curve. Reported roughness values were found to vary by <7% over three spots on each film.

Electrical resistivity measurements were performed on a Quantum Design DynaCool Physical Property Measurement System (PPMS). The TiN films were connected to the PPMS sample holder by four aluminum wires, wirebonded with a Westbond 7476D Wire Bonder. The film resistivity (ρ) was measured using a four-point setup.[7] The resistivity was measured from 6 to 1.7 K, and the data were used to calculate the superconducting critical temperature (T_c) of the films.

The samples consisted of 50 and 60 nm thick TiN films on high resistivity Si (100) wafers (> 20 kΩcm, UniversityWafer) prepared using ALD with the same FlexAL system. The ALD process consisted of sequential half-cycles of exposure to tetrakis(dimethylamino)titanium (TDMAT) and nitrogen plasma with a 20 W DC bias at 350 °C, similar to the procedure reported in Refs. 7 and 57. The resistance at 6 K and T_c of a 60 nm thick ALD TiN film were measured to be 210 $\mu\Omega$cm and 3.22 ± 0.06 K, respectively; these values are comparable to those reported for other TiN films made using TDMAT.[7,57,58] The chemical composition of the deposited films is described in Sec. III E. The titania (TiO_2) films used for demonstrating etch selectivity in Sec. III A were made by oxidizing TiN samples under an oxygen plasma for 5 min at 300 °C, yielding a 5 nm thick TiO_2 film on top of the TiN film. The thicknesses of the TiO_2 films were measured using *ex situ* ellipsometry.

III. RESULTS

A. Selective etching with SF_6/H_2 plasma

We begin by examining the etch rate of TiO_2 and TiN films for various SF_6:H_2 flow rate ratios, η. Figure 2(a) shows the etch

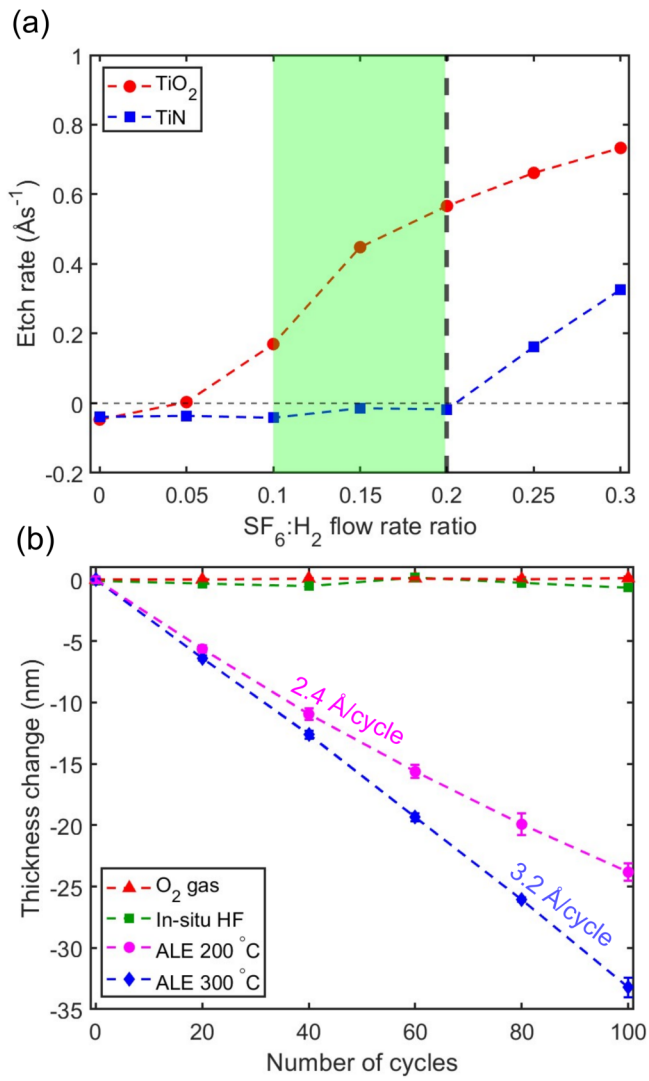

FIG. 2. (a) Etch rate of TiO_2 (red circles) and TiN (blue squares) vs the SF_6:H_2 flow rate ratio. The green shaded area represents the flow rate ratios for which selective etching of TiO_2 over TiN was achieved. The vertical dashed black line at a ratio of 0.2 represents the ratio used in the ALE experiments. (b) TiN thickness change vs number of cycles with exposure only to O_2 gas (red triangles), *in situ* HF (green squares), full ALE process at 200 °C (purple circles), and 300 °C (blue diamonds). The dashed lines are guides to the eye.

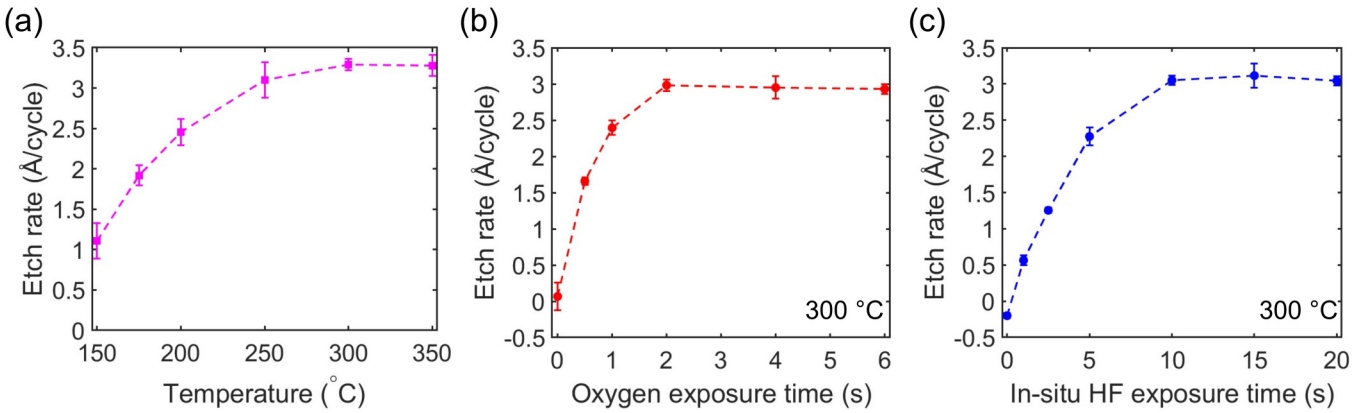

FIG. 3. (a) TiN ALE etch per cycle (EPC) vs substrate table temperature. (b) EPC vs O_2 gas exposure time with *in situ* HF exposure time fixed at 10 s at 300 °C. (c) EPC vs *in situ* HF time with O_2 exposure time fixed at 2 s at 300 °C. The etch rates are observed to saturate with exposure time, demonstrating the self-limiting nature of the ALE process. The dashed lines are guides to the eye.

rates of TiN and TiO_2 versus η at 300 °C. For $\eta \lesssim 0.05$, negligible etching of either film is observed. At $\eta = 0$, we measure an etch rate of −0.03 Å/cycle. This value is within the measurement error of the ellipsometer, and as such, we do not attribute physical significance to the negative value. The other negative etch rates correspond to an increase in the thickness of the film, which we assume to be growth of nonvolatile TiF_3. For $\eta \geq 0.1$, we observe spontaneous etching of TiO_2, with the etch rate monotonically increasing with η. For TiN, we observe no etching for $\eta \leq 0.2$, but for $\eta \geq 0.25$, etching occurs. We attribute these observations to the formation of *in situ* HF along with negligible fluorine radical concentration for $0.05 < \eta \leq 0.2$. For $\eta \geq 0.25$, the concentration of F radicals becomes sufficient to spontaneously etch the TiN, leading to increasing etch rates for both films. From our measurements, we find that $0.1 \leq \eta \leq 0.2$ achieves selective etching of TiO_2 over TiN. To obtain the highest etch selectivity of TiO_2 over TiN, we select $\eta = 0.2$ for our experiments. This 1:5 ratio of SF_6:H_2 plasma is used throughout the rest of the paper.

B. TiN ALE using O_2 and *in situ* HF exposures

Figure 3(b) shows the thickness change of TiN versus number of cycles for both half-cycles and for the full ALE recipe at 200 °C and 300 °C. For the half-cycles, the thickness change was measured after exposure to only molecular oxygen or *in situ* HF. No etching was observed for either half-cycle. In contrast, we observe a decrease in the thickness with increasing number of cycles when using both steps. The etch rate is calculated by dividing the total thickness change by the number of cycles, giving values of 2.4 ± 0.16 Å/cycle at 200 °C and 3.2 ± 0.10 Å/cycle at 300 °C.

We further examine the effect of temperature on the etch rate. Figure 3(a) shows the EPC versus table temperature ranging from 150 °C to 350 °C. The etch rates are calculated from the thickness change over 100 cycles. We find that the etch rate increases from 1.1 Å/cycle at 150 °C to 3.2 Å/cycle at 300 °C. In analogy to other works,[18,43,44] we attribute the etch rate increase with temperature to the higher diffusion rates at higher temperatures in the oxidation step, leading to thicker oxides, which are etched at each step. We also observe a constant etch rate from 300 °C to 350 °C, similar to what is reported in Fig. 7 of Ref. 43.

We also explored the self-limiting nature of the process by measuring the saturation curves of each half-cycle. For each saturation curve, the temperature is set to 300 °C, and the purge times and one half-cycle time are fixed while the other is varied. In Fig. 3(b), the *in situ* HF step is fixed at 10 s, while the etch rate is measured versus the oxygen exposure time. The etch rate is observed to saturate to ∼3 Å/cycle above 2 s, which is consistent with the self-limiting nature of the oxidation step. In Fig. 3(c), the oxidation step is fixed at 2 s, while the etch rate is measured versus *in situ* HF exposure time. The etch rate saturates to ∼3 Å/cycle above 10 s, which is consistent with the selectivity of the *in situ* HF to etch TiO_2 and terminate on the TiN.

C. Characterization of film composition

We next characterize the chemical composition of the TiN films before and after ALE using XPS. In Fig. 4, we show the core levels of Ti2p, N1s, O1s, C1s, and F1s. For the Ti2p XPS spectra in Fig. 4(a), we observe five components. Each component is a doublet consisting of a $2p_{3/2}$ and $2p_{1/2}$ subpeak. We observe subpeaks corresponding to Ti–C (454.9 and 460.4 eV),[59–61] Ti–N (455.1 and 460.8 eV),[62–64] Ti–ON (456.5 and 462.3 eV),[62–64] Ti–O (458.5 and 464.2 eV),[62–64] and Ti–F (459.4 and 465.6 eV).[65,66] In Fig. 4(b), we report the N1s spectra with two subpeaks at 397.1 and 398.9 eV, belonging to N–Ti and N–O bonds, respectively.[62–64] In Fig. 4(c), we report the O1s spectra with two subpeaks at 530.4 eV and 532.2 eV, corresponding to O–Ti and O–N bonds, respectively.[62–64] In Fig. 4(d), we report the F1s spectra with two subpeaks at 684.9 and 690.3 eV, corresponding to F–Ti and F–C bonds, respectively.[65–67]

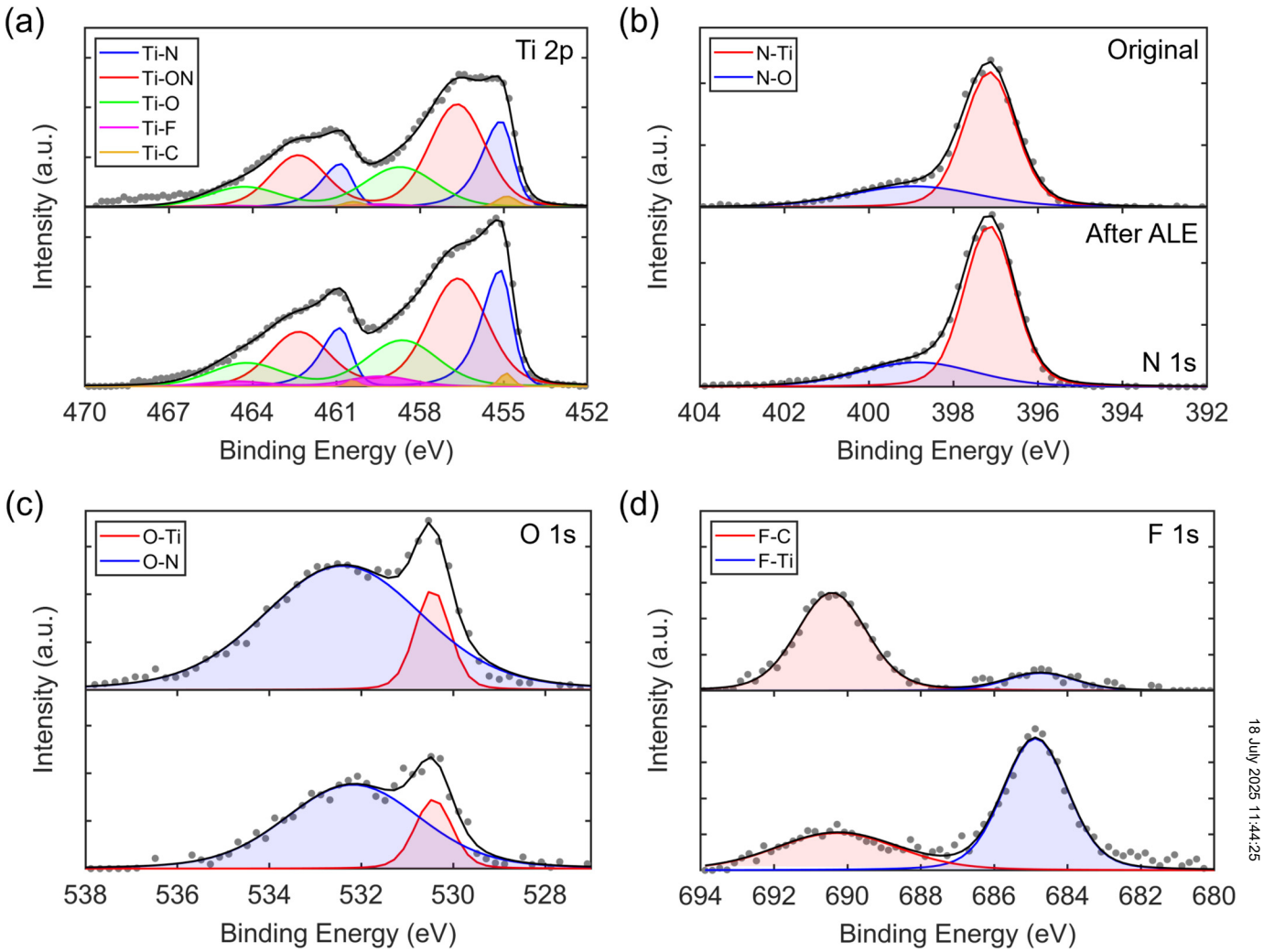

FIG. 4. Surface XPS spectra showing (a) Ti2p, (b) N1s, (c) O1s, and (d) F1s spectra. The spectra are shown for (top) original and (bottom) etched TiN films. The measured (gray dots) and fit spectra (black lines) intensities are reported in arbitrary units (a.u.) against the binding energy on the *x* axis. The *y* axis scale is identical between panels within each subfigure.

We observe that the Ti2p spectra are dominated by oxides and oxynitrides, consistent with the presence of a native oxide on TiN.[58,63] After ALE [bottom panels of Figs. 4(a)–4(c)], an increase in the magnitude of the Ti–N and N–Ti peaks is observed along with an overall decrease in the O1s peak magnitude. The decreased O1s signal implies reduced native oxide concentration after ALE, as has been observed in ALE of other materials.[33,68,69] The F1s spectra for the original sample may be attributed to contamination from using the same chamber for deposition and etching, which is consistent with the reduced magnitude of the F1s peak in the original sample compared to that in the ALE-treated sample [bottom panel of Fig. 4(d)].

We also performed depth-profiling XPS to determine the atomic concentrations on the surface and in the bulk. In Fig. 5, we show the atomic concentrations of Ti, N, F, C, and O versus sputtering time and estimated depth in the original and ALE-treated films. In the original sample [Fig. 5(a)], the atomic concentrations on the surface are 31.9% (Ti), 37.6% (N), 16.1% (O), 12.0% (C), and 2.4% (F). After 120 s Ar milling (~3.5 nm), the atomic concentrations plateau to their bulk values of 48.6% (Ti), 42.3% (N), 6.1% (O), 1.9% (C), and 1.1% (F). The carbon and oxygen levels are consistent with other reported ALD TiN films made using TDMAT.[58,70,71] The carbon signal on the surface is observed to be predominantly C–O and C–H bonds, expected from adventitious

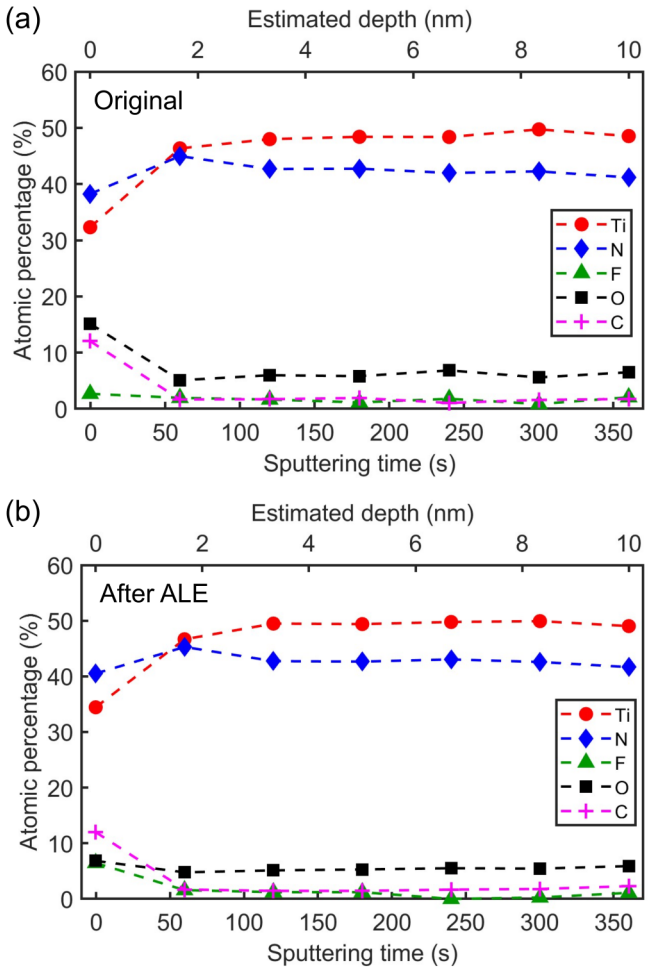

FIG. 5. Atomic concentrations of Ti, N, O, F, and C vs Ar milling time and estimated depth for (a) original and (b) ALE-treated TiN thin films. The dashed lines are guides to the eye.

carbon, which occurs on exposure to atmosphere. The carbon signal in the bulk is from C–Ti bonds, which has been attributed to the decomposition of TDMAT during ALD in prior studies.[58] The carbon and oxygen contamination in the bulk is known to cause higher resistivities and lower T_c compared to films with lower contamination concentrations.[58,72] For the ALE-treated sample [Fig. 5(b)], the atomic concentrations on the surface are 34.2% (Ti), 39.5% (N), 7.9% (O), 11.9% (C), and 6.5% (F). After 120 s Ar milling (~3.5 nm), the atomic concentrations plateau to their bulk values of 49.0% (Ti), 42.2% (N), 5.9% (O), 1.8% (C), and 1.1% (F). We observe a ~49% decrease in the surface oxygen concentration in the ALE-treated film. An increase in the surface fluorine concentration of the ALE-treated film is also observed, consistent with other works involving the interactions of fluorine-containing plasma with dielectric films.[33,68,73] The atomic concentrations in the bulk of the ALE-treated film are within 95% of the values in the original film. Therefore, we conclude that the effect of ALE is confined to a few nanometers of the surface, with negligible effect on the bulk chemical composition.

D. Surface roughness characterization

We characterized the roughness of the TiN films before and after ALE using AFM. Figure 6(a) shows the plane-fit height map of the film as deposited using ALD. Figure 6(b) shows the plane-fit height map after 100 cycles of ALE at 300 °C. Figure 6(c) shows the PSD curves for the original film, after 40 ALE cycles and after 100 ALE cycles at 300 °C. We observe a decrease in the PSD intensity across all length scales as the number of ALE cycles is increased, indicating that features with length scales from $\sim 2-20$ nm are smoothed by the ALE process. In Fig. 6(d), the RMS roughness is plotted versus the number of ALE cycles at 300 °C. We observe a monotonic decrease in RMS roughness from 4.4 to 2.5 Å after 100 cycles. This 43% reduction in roughness was observed across three different positions on the sample.

E. Electrical and superconducting properties

We investigated the effect of ALE on the electrical and superconducting properties of the TiN films by measuring their resistivity from 6 to 1.7 K. A 60 nm TiN film was deposited using ALD, which was etched to 50 nm using ALE. Another 50 nm TiN film was prepared using ALD to compare to the ALE-treated 50 nm film. The measured resistivity versus temperature for the three films is shown in Fig. 7. The resistivity at 6 K of the 60 nm ALD film is found to be 222 $\mu\Omega$cm, with a superconducting critical temperature $T_c = 3.22 \pm 0.06$ K. The resistivity of the TiN film is consistent with those previously reported for ALD TiN films,[7,58] and the T_c reported is similar to T_c of other TiN films grown with TDMAT.[7,72] After 40 cycles of ALE at 200 °C, the TiN thickness decreased to 50 nm, with a resistivity of 201 $\mu\Omega$cm at 6 K and $T_c = 3.13 \pm 0.04$ K. For comparison, the 50 nm ALD film had a resistivity of 227 $\mu\Omega$cm at 6 K and $T_c = 3.11 \pm 0.05$ K. We, therefore, find that the change in T_c of the TiN film after ALE is consistent with that expected with a decrease of 10 nm in thickness, without any additional decrease due to process-induced damage. This observation highlights the improved quality of the processed films compared to those obtained from processing methods, which lack atomic control. For example, nitrogen plasma treatment of Nb films resulted in a T_c decrease of ~9%.[74] The reduced resistivity at 6 K of the ALE-treated film is thought to arise due to the removal of the native oxide. To test this hypothesis, the ALE-treated film's electrical properties were measured after two months in ambient atmosphere. The resistivity at 6 K and T_c were measured as 214 $\mu\Omega$cm and 3.09 ± 0.02 K, respectively. The T_c change is within the uncertainty of the initial ALE-treated film's T_c of 3.13 ± 0.04 K. The aged resistivity increased from 201 $\mu\Omega$cm, as expected due to reoxidation of the film after ALE with exposure to atmosphere. However, the resistivity did not increase to the value of the 50 nm ALD film (227 $\mu\Omega$cm). We hypothesize that the lower resistivity of the ALE-treated sample is due to the fluorinated surface serving as a diffusion barrier for oxygen, similar

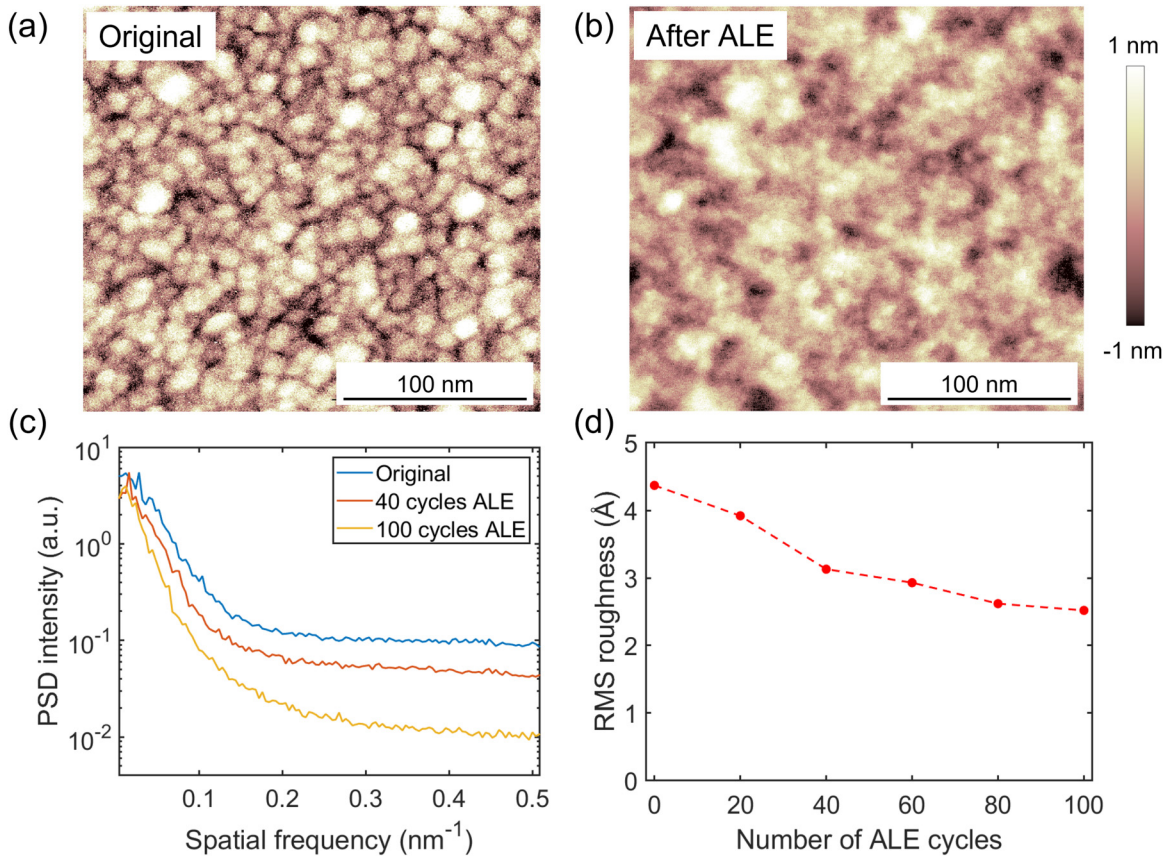

FIG. 6. AFM scan showing height maps of an original ALD sample (a) and after 100 ALE cycles (b). (c) Height map PSD versus spatial frequency for varying number of ALE cycles, showing a decrease in PSD intensity across all spatial frequencies with increasing number of cycles. (d) RMS roughness computed from an AFM height map against the number of ALE cycles. The dashed line is a guide to the eye.

to the effect observed in Ref. 68. These results warrant further investigation and is a topic of future study.

IV. DISCUSSION

We now discuss the characteristics of our plasma-thermal TiN ALE process in context with isotropic thermal ALE processes for TiN and related materials. Thermal ALE of TiN has been reported using molecular O_3 or H_2O_2 and HF vapor,[43] and O_2 plasma and CF_4 plasma.[44] The first process leads to an EPC of 0.20 Å/cycle at 200 °C, achieving atomic-scale control of etching. However, the recipe requires the use of HF vapor, which incurs practical complications. The second process based on O_2 plasma and CF_4 plasma achieves an EPC of 17.1 Å/cycle at 200 °C, which is a larger EPC than is desired for manipulating the surface region of the films. The second process also requires an additional heating step, which can lead to impractical process times on conventional tools. The present recipe achieves an EPC of 2.4 Å/cycle at 200 °C, providing etch rates between the previous reported recipes. The present recipe also avoids the use of HF, requiring only an SF_6/H_2 plasma that yields etching selectivity of TiO_2 over TiN.

Our isotropic plasma-thermal ALE may find potential applications in the fabrication of TiN-based superconducting microresonators for microwave kinetic inductance detectors and qubits, where the native oxide hosts parasitic TLS that presently limit the device performance. Based on our XPS and resistivity measurements, ALE-treated films have reduced oxygen concentration while maintaining unaltered bulk chemistry and electrical properties. These properties make ALE promising for reducing the number of TLS in the metal-air interface and, therefore, improving the quality factor of superconducting microresonators. While isotropic etching is less suitable for pattern transfer compared to anisotropic etching, isotropic ALE may find application as a post-treatment process by removing the few-nanometer-thick surface region hosting TLS after the primary etch process. The smoothing effect and the isotropic angstrom-scale EPC of the present ALE recipe are also relevant for fabricating TiN-based nanoscale metal gate electrodes in CMOS devices and various transistor designs, where the metal layers are required to have thickness on the order of ∼10 nm with uniformity

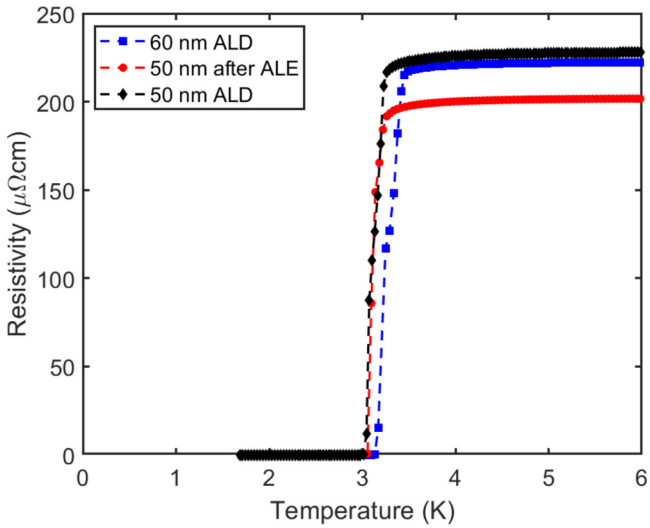

FIG. 7. Resistivity vs temperature for an original 60 nm TiN film (blue squares), an ALE-treated film of 50 nm thickness (red circles), and a 50 nm ALD TiN film (black diamonds) for comparison. The difference in T_c between the 50 nm ALD film and the ALE-treated 50 nm film is negligible. The dashed lines are guides to the eye.

$\lesssim 4\%$.[9,75] The ALD system in our work (Oxford Instruments, FlexAL) has demonstrated high uniformity on 200 mm diameter substrates,[51] and therefore, our process has the potential to extend to wafer-scale applications.

V. CONCLUSION

We have reported an isotropic plasma-thermal atomic layer etching process for TiN using sequential exposures of molecular oxygen and SF_6/H_2 plasma. The SF_6/H_2 plasma selectively etches TiO_2 over TiN for SF_6:H_2 flow rate ratios between 0.1 and 0.2. The etch rate varies from 1.1 Å/cycle at 150 °C to 3.2 Å/cycle at 350 °C. We observe a smoothing effect from ALE, corresponding to a ~43% reduction in RMS roughness after 100 cycles. The surface oxygen concentration is reduced by ~49% after 100 cycles of ALE, indicating a decrease in the volume of surface oxide. We also find that ALE does not induce any change in T_c beyond that expected from the decrease in film thickness, highlighting the low-damage nature of the process. We anticipate that the ability to engineer the surface of TiN films on the angstrom-scale using isotropic ALE will facilitate applications of TiN in superconducting resonators and microelectronics.

ACKNOWLEDGMENTS

This work was supported by NSF under Award No. 2234390. The authors thank Nicholas Chittock (Eindhoven University of Technology) for useful discussions and Phillipe Pearson (California Institute of Technology) for assistance with the wirebonder. We gratefully acknowledge the critical support and infrastructure provided for this work by The Kavli Nanoscience Institute and the Molecular Materials Research Center of the Beckman Institute at the California Institute of Technology.

AUTHOR DECLARATIONS

Conflict of Interest

The authors have no conflicts to disclose.

Author Contributions

Azmain A. Hossain: Conceptualization (equal); Data curation (lead); Formal analysis (lead); Investigation (equal); Methodology (equal); Validation (equal); Visualization (equal); Writing – original draft (lead); Writing – review & editing (lead). **Haozhe Wang:** Data curation (supporting); Formal analysis (supporting); Investigation (supporting). **David S. Catherall:** Data curation (supporting); Formal analysis (supporting); Investigation (supporting); Methodology (equal); Writing – review & editing (supporting). **Martin Leung:** Data curation (supporting); Formal analysis (supporting). **Harm C. M. Knoops:** Conceptualization (equal); Methodology (equal); Writing – review & editing (equal). **James R. Renzas:** Conceptualization (equal); Methodology (equal); Writing – review & editing (equal). **Austin J. Minnich:** Conceptualization (equal); Formal analysis (equal); Funding acquisition (lead); Investigation (lead); Methodology (equal); Project administration (lead); Resources (lead); Supervision (lead); Validation (lead); Visualization (lead); Writing – original draft (lead); Writing – review & editing (lead).

DATA AVAILABILITY

The data that support the findings of this study are available from the corresponding author upon reasonable request.

REFERENCES

[1]H. G. Leduc *et al.*, Appl. Phys. Lett. **97**, 102509 (2010).
[2]M. R. Vissers, J. Gao, D. S. Wisbey, D. A. Hite, C. C. Tsuei, A. D. Corcoles, M. Steffen, and D. P. Pappas, Appl. Phys. Lett. **97**, 232509 (2010).
[3]A. Kher, P. K. Day, B. H. Eom, J. Zmuidzinas, and H. G. Leduc, J. Low Temp. Phys. **184**, 480 (2016).
[4]B. Ho Eom, P. K. Day, H. G. LeDuc, and J. Zmuidzinas, Nat. Phys. **8**, 623 (2012).
[5]T. M. Hazard, A. Gyenis, A. Di Paolo, A. T. Asfaw, S. A. Lyon, A. Blais, and A. A. Houck, Phys. Rev. Lett. **122**, 010504 (2019).
[6]J. B. Chang *et al.*, Appl. Phys. Lett. **103**, 012602 (2013).
[7]A. Shearrow, G. Koolstra, S. J. Whiteley, N. Earnest, P. S. Barry, F. J. Heremans, D. D. Awschalom, E. Shirokoff, and D. I. Schuster, Appl. Phys. Lett. **113**, 212601 (2018).
[8]H. Kim, J. Vac. Sci. Technol. B **21**, 2231 (2003).
[9]C. Zhao and J. Xiang, Appl. Sci. **9**, 2388 (2019).
[10]L. P. B. Lima, M. A. Moreira, J. A. Diniz, and I. Doi, Phys. Status Solidi C **9**, 1427 (2012).
[11]J. Gao, J. Zmuidzinas, B. A. Mazin, H. G. LeDuc, and P. K. Day, Appl. Phys. Lett. **90**, 102507 (2007).
[12]R. Barends, H. L. Hortensius, T. Zijlstra, J. J. A. Baselmans, S. J. C. Yates, J. R. Gao, and T. M. Klapwijk, Appl. Phys. Lett. **92**, 223502 (2008).
[13]J. Gao, M. Daal, A. Vayonakis, S. Kumar, J. Zmuidzinas, B. Sadoulet, B. A. Mazin, P. K. Day, and H. G. Leduc, Appl. Phys. Lett. **92**, 152505 (2008).
[14]M. Sandberg, M. R. Vissers, J. S. Kline, M. Weides, J. Gao, D. S. Wisbey, and D. P. Pappas, Appl. Phys. Lett. **100**, 262605 (2012).
[15]M. V. P. Altoé *et al.*, PRX Quant. **3**, 020312 (2022).

[16]R. Gao, W. Yu, H. Deng, H.-S. Ku, Z. Li, M. Wang, X. Miao, Y. Lin, and C. Deng, Phys. Rev. Mater. **6**, 036202 (2022).
[17]T. Lill, K. J. Kanarik, S. Tan, M. Shen, E. Hudson, Y. Pan, J. Marks, V. Vahedi, and R. A. Gottscho, in *Encyclopedia of Plasma Technology* (CRC Press, Boca Raton, FL, 2016), pp. 133–142.
[18]S. M. George, Acc. Chem. Res. **53**, 1151 (2020).
[19]X. Sang, Y. Xia, P. Sautet, and J. P. Chang, J. Vac. Sci. Technol. A **38**, 043005 (2020).
[20]H. Sakaue, S. Iseda, K. Asami, J. Yamamoto, M. Hirose, and Y. Horiike, Jpn. J. Appl. Phys. **29**, 2648 (1990).
[21]Y. Horiike, T. Tanaka, M. Nakano, S. Iseda, H. Sakaue, A. Nagata, H. Shindo, S. Miyazaki, and M. Hirose, J. Vac. Sci. Technol. A **8**, 1844 (1990).
[22]K. J. Kanarik, T. Lill, E. A. Hudson, S. Sriraman, S. Tan, J. Marks, V. Vahedi, and R. A. Gottscho, J. Vac. Sci. Technol. A **33**, 020802 (2015).
[23]G. S. Oehrlein, D. Metzler, and C. Li, ECS J. Solid State Sci. Technol. **4**, N5041 (2015).
[24]S. M. George and Y. Lee, ACS Nano **2016**, 5 (2016).
[25]N. Miyoshi, H. Kobayashi, K. Shinoda, M. Kurihara, T. Watanabe, Y. Kouzuma, K. Yokogawa, S. Sakai, and M. Izawa, Jpn. J. Appl. Phys. **56**, HB0106 (2017).
[26]E.-J. Song, J.-H. Kim, J.-D. Kwon, S.-H. Kwon, and J.-H. Ahn, Jpn. J. Appl. Phys. **57**, 106505 (2018).
[27]K. Osakada, in *Current Methods in Inorganic Chemistry* (Elsevier, Waltham, MA, 2003), Vol. 3, pp. 233–291.
[28]D. R. Zywotko, J. Faguet, and S. M. George, J. Vac. Sci. Technol. A **36**, 061508 (2018).
[29]Y. Lee, J. W. DuMont, and S. M. George, Chem. Mater. **27**, 3648 (2015).
[30]J. W. DuMont, A. E. Marquardt, A. M. Cano, and S. M. George, ACS Appl. Mater. Interfaces **9**, 10296 (2017).
[31]R. Rahman, E. C. Mattson, J. P. Klesko, A. Dangerfield, S. Rivillon-Amy, D. C. Smith, D. Hausmann, and Y. J. Chabal, ACS Appl. Mater. Interfaces **10**, 31784 (2018).
[32]N. R. Johnson, H. Sun, K. Sharma, and S. M. George, J. Vac. Sci. Technol. A **34**, 050603 (2016).
[33]H. Wang, A. Hossain, D. Catherall, and A. J. Minnich, J. Vac. Sci. Technol. A **41**, 032606 (2023).
[34]A. M. Cano, A. Lii-Rosales, and S. M. George, J. Phys. Chem. C **126**, 6990 (2022).
[35]W. Lu, Y. Lee, J. C. Gertsch, J. A. Murdzek, A. S. Cavanagh, L. Kong, J. A. del Alamo, and S. M. George, Nano Lett. **19**, 5159 (2019).
[36]T. Ohba, W. Yang, S. Tan, K. J. Kanarik, and K. Nojiri, Jpn. J. Appl. Phys. **56**, 06HB06 (2017).
[37]Y. Lee, J. W. DuMont, and S. M. George, ECS J. Solid State Sci. Technol. **4**, N5013 (2015).
[38]C. Fang, Y. Cao, D. Wu, and A. Li, Prog. Nat. Sci.: Mater. Int. **28**, 667 (2018).
[39]A. Fischer, A. Routzahn, S. M. George, and T. Lill, J. Vac. Sci. Technol. A **39**, 030801 (2021).
[40]K. J. Kanarik *et al.*, J. Vac. Sci. Technol. A **35**, 05C302 (2017).
[41]S. H. Gerritsen, N. J. Chittock, V. Vandalon, M. A. Verheijen, H. C. M. Knoops, W. M. M. Kessels, and A. J. M. Mackus, ACS Appl. Nano Mater. **5**, 18116 (2022).
[42]Y. Lee, C. Huffman, and S. M. George, Chem. Mater. **28**, 7657 (2016).
[43]Y. Lee and S. M. George, Chem. Mater. **29**, 8202 (2017).
[44]D. Shim, J. Kim, Y. Kim, and H. Chae, J. Vac. Sci. Technol. B **40**, 022208 (2022).
[45]S. J. Pearton, A. Katz, and A. Feingold, Semicond. Sci. Technol. **6**, 830 (1991).
[46]V. Volynets, Y. Barsukov, G. Kim, J.-E. Jung, S. K. Nam, K. Han, S. Huang, and M. J. Kushner, J. Vac. Sci. Technol. A **38**, 023007 (2020).
[47]J.-E. Jung, Y. Barsukov, V. Volynets, G. Kim, S. K. Nam, K. Han, S. Huang, and M. J. Kushner, J. Vac. Sci. Technol. A **38**, 023008 (2020).
[48]P. A. Pankratiev, Y. V. Barsukov, A. A. Kobelev, A. Y. Vinogradov, I. V. Miroshnikov, and A. S. Smirnov, J. Phys. Conf. Ser. **1697**, 012222 (2020).
[49]N. J. Chittock, M. F. J. Vos, T. Faraz, W. M. M. Kessels, H. C. M. Knoops, and A. J. M. Mackus, Appl. Phys. Lett. **117**, 162107 (2020).
[50]P. C. J. J. Coumou, M. R. Zuiddam, E. F. C. Driessen, P. J. de Visser, J. J. A. Baselmans, and T. M. Klapwijk, IEEE Trans. Appl. Supercond. **23**, 7500404 (2012).
[51]J. L. van Hemmen, S. B. S. Heil, J. H. Klootwijk, F. Roozeboom, C. J. Hodson, M. C. M. van de Sanden, and W. M. M. Kessels, J. Electrochem. Soc. **154**, G165 (2007).
[52]E. Langereis, S. B. S. Heil, M. C. M. van de Sanden, and W. M. M. Kessels, J. Appl. Phys. **100**, 023534 (2006).
[53]D. Jaeger and J. Patscheider, J. Electron Spectrosc. Relat. Phenom. **185**, 523 (2012).
[54]M. Maarouf, M. B. Haider, Q. A. Drmosh, and M. B. Mekki, Crystals **11**, 239 (2021).
[55]T. D. B. Jacobs, T. Junge, and L. Pastewka, Surf. Topogr. Metrol. Prop. **5**, 013001 (2017).
[56]J. M. Elson and J. M. Bennett, Appl. Opt. **34**, 201 (1995).
[57]T. Faraz *et al.*, ACS Appl. Mater. Interfaces **10**, 13158 (2018).
[58]J. Musschoot, Q. Xie, D. Deduytsche, S. Van den Berghe, R. L. Van Meirhaeghe, and C. Detavernier, Microelectron. Eng. **86**, 72 (2009).
[59]F. Santerre, M. A. El Khakani, M. Chaker, and J. P. Dodelet, Appl. Surf. Sci. **148**, 24 (1999).
[60]L.-Å. Näslund, P. O. Å. Persson, and J. Rosen, J. Phys. Chem. C **124**, 27732 (2020).
[61]J. Luthin and Ch. Linsmeier, Phys. Scr. **91**, 134 (2001).
[62]M. V. Kuznetsov, Ju. F. Zhuravlev, V. A. Zhilyaev, and V. A. Gubanov, J. Electron Spectrosc. Relat. Phenom. **58**, 1 (1992).
[63]N. C. Saha and H. G. Tompkins, J. Appl. Phys. **72**, 3072 (1992).
[64]M.-H. Chan and F.-H. Lu, Thin Solid Films **517**, 5006 (2009).
[65]C. Mousty-Desbuquoit, J. Riga, and J. J. Verbist, Inorg. Chem. **26**, 1212 (1987).
[66]V. Natu, M. Benchakar, C. Canaff, A. Habrioux, S. Célérier, and M. W. Barsoum, Matter **4**, 1224 (2021).
[67]G. Beamson and D. Briggs, High resolution XPS of organic polymers: The Scienta ESCA300 database," J. Chem. Educ. **70**(1), A25 (1993).
[68]J. Hennessy, C. S. Moore, K. Balasubramanian, A. D. Jewell, K. France, and S. Nikzad, J. Vac. Sci. Technol. A **35**, 041512 (2017).
[69]D. Metzler, C. Li, C. S. Lai, E. A. Hudson, and G. S. Oehrlein, J. Phys. D: Appl. Phys. **50**, 254006 (2017).
[70]F. Fillot, T. Morel, S. Minoret, I. Matko, S. Maîtrejean, B. Guillaumot, B. Chenevier, and T. Billon, Microelectron. Eng. **82**, 248 (2005).
[71]J. W. Elam, M. Schuisky, J. D. Ferguson, and S. M. George, Thin Solid Films **436**, 145 (2003).
[72]T. Proslier, J. Klug, N. C. Becker, J. W. Elam, and M. Pellin, ECS Trans. **41**, 237 (2011).
[73]A. Fischer, R. Janek, J. Boniface, T. Lill, K. J. Kanarik, Y. Pan, V. Vahedi, and R. A. Gottscho, Proc. SPIE **10149**, 101490H (2017).
[74]K. Zheng, D. Kowsari, N. J. Thobaben, X. Du, X. Song, S. Ran, E. A. Henriksen, D. S. Wisbey, and K. W. Murch, Appl. Phys. Lett. **120**, 102601 (2022).
[75]T. Matsukawa, K. Endo, H. Akasaka, Y. Kamiya, M. Ikeda, K. Tsunekawa, T. Nakagawa, Y. X. Liu, and M. Masahara, *2015 Silicon Nanoelectronics Workshop (SNW)*, Kyoto, Japan, 14–15 June 2015 (IEEE, Tokyo, Japan, 2015), pp. 1–2.